

Article

# A Fractional-Order Element (FOE)-Based Approach to Wireless Power Transmission for Frequency Reduction and Output Power Quality Improvement

Guidong Zhang <sup>1</sup>, Zuhong Ou <sup>1</sup> and Lili Qu <sup>2,\*</sup>

<sup>1</sup> School of Automation, Guangdong University of Technology, Guangzhou 510006, China;  
guidong.zhang@gdut.edu.cn (G.Z.); zuhong.ou@foxmail.com (Z.O.)

<sup>2</sup> School of Automation, Foshan University, Foshan 528225, China

\* Correspondence: qulili@fosu.edu.cn; Tel.: +86-139-2590-6648

Received: 3 September 2019; Accepted: 11 September 2019; Published: 13 September 2019



**Abstract:** A wireless power transmission (WPT) requires high switching frequency to achieve energy transmission; however, existing switching devices cannot satisfy the requirements of high-frequency switching, and the efficiency of current WPT is too low. Compared with the traditional power inductors and capacitors, fractional-order elements (FOEs) in WPT can realize necessary functions through requiring a lower switching frequency, which leads to a more favorable high-frequency switching performance with a higher efficiency. In this study, a generalized fractional-order WPT (FO-WPT) is established, followed by a comprehensive analysis on its WPT performance and power efficiency. Through extensive simulations of typical FO wireless power domino-resonators (FO-WPDRS), the functionality of the proposed FO-WPT for medium and long-range WPT is demonstrated. The numerical results show that the proposed FOE-based WPT solution has a higher power efficiency and lower switching frequency than conventional methods.

**Keywords:** fractional order elements; high-frequency switching; wireless power transmission

---

## 1. Introduction

Wireless power transmission (WPT) is gaining more and more attention in city transportation applications since *Tesla* firstly revealed WPT in the 1880s [1]. It is also revealed that WPT is of great practical significance due to its immunity to fire and electric shock [2]. Recently, the most extensive studies in WPT are inductive coupling WPT (ICWPT), magnetic resonance coupling WPT (MRCWPT) and microwave wireless power transmission (MWPT) [3]. Compared with ICWPT, MRCWPT transfers power over a longer distance and powers several multiple loads via a single transmitter coil simultaneously [4]. Among three techniques mentioned above, MWPT's (also named as radio frequency-based WPT) efficiency is the lowest one but its transfer distance is longest [5,6]. Therefore, when *Soljačić* with the Massachusetts Institute of Technology (MIT) successfully lit up a bulb over 2 m with 40% energy efficiency in 2007 [7], MRCWPT stimulated international research.

In [8], the authors propose a simple method for the analysis of the resonance frequency of a planar spiral coil to evaluate the lumped parameters of the coils. Using the technology of electromagnetic resonant couplings WPT [9], the authors addressed the fact that the output power can reach 100 W. Ref. [10] showed that magnetic resonant coupling WPT normally works in megahertz and its efficiency is improved with increasing frequency. Despite its long-lasting popularity, using coils to achieve WPT through high-frequency actions cannot satisfy today's needs, and power electronics elements are being developed to realize the same function [11]. However, it is well known that current power electronics technologies cannot satisfy such high-frequency switching [12]; therefore, in order to meet

the capability of contemporary power switches to realize WPT, it is of great necessity to propose new methods for reducing the resonant frequency. Traditionally, a pair of coil resonators were applied to mid- and long-range wireless power transfer, but this technique has a poor performance in energy transfer efficiency [13]. To solve this problem, a new method of using coil arrays at both the transmitter and receiver sides was introduced employing the technique of mid-range strong magnetic resonant coupling [14]. Although the transmission separation is 50 cm, its efficiency of the system is 50% and it is still too low. Another new method is to determine a model for coupling coefficient to compute optimal frequency for the power transfer [15]. To overcome this problem, relay resonators, which are normally used in meta-materials and waveguide research [16], were implemented into WPT for mid-range or even long-range wireless power transfer [17]. Inspired by this idea, the domino resonators for waveguide applications at 100 MHz have been reported in [18]; however, the switching frequency is too high for existing power electronics elements. Zhong found that cross-coupling effects of non-adjacent resonators can both improve the efficiency and reduce the switching frequency at 520 kHz resulting from the effects of the magnetic coupling of non-adjacent resonators [19]. In contrast to Zhong's strategy, a WPT system which was designed using superconducting coils to boost wireless power transmission efficiency offered higher transmission efficiency at a longer distance [20]. However, this method is not practical because of the high economic cost and difficulty in realizing the superconducting coils [21]. Please note that WPT's resonant frequency is still very high via current power converter technology. Therefore, a methodology is eagerly required to further reduce the frequency and improve the output power and efficiency.

To well solve the aforementioned problems, an optimizable circuit structure was developed in [22], achieving 85% transfer efficiency at a distance of 10 cm and 50% at 20 cm. It is obvious that they solved the problem by tuning parameters with an optimized model, which nonetheless did not resolve the problem at a fundamental level [23]. Therefore, it still lacks a methodology to realize maximum efficiency and obtain other favorable output features.

Recently, Fractional-Order Electrical Elements (FOE) were applied to electrical engineering applications. In general, two elements are required for impedance matching networks of integer circuit, while only a single FOE is required for fractional cases [24,25] since it has the feature of an extra degree-of-freedom to realize functions of both inductors and capacitors. For example, fractional-order capacitor (FOC) with  $1 < \alpha < 2$  ( $\alpha$  is the order of the FOC) can be used to improve output power features and decrease the resonant frequency [26,27]. In fact, these unique features of FOEs are needed for the applications of WPT. Furthermore, an FOE is mostly constructed into a ladder network consisting of resistors and capacitors (or inductors) [28], which demonstrates that implementation of FOE costs little; however, this still lacks some fundamental studies.

To reduce resonant frequency and improve the output power and efficiency of WPT, this paper proposes a novel WPT implemented with FOEs, which we brand FO-WPT. A typical example, wireless power domino-resonators, or FO-WPDRS, is presented to confirm the flexibility and versatility of the proposed solution. The remainder of this paper is organized as follows. Fundamental analysis and introduction of FOEs are presented in Section 2. It is followed up with modelling of FO-WPT in Section 3. In order to verify this idea, FO-WPDRS is analyzed as an example with detailed derivations of output power and transmission efficiency in Section 4. Compared with WPDRS, the unique features of the proposed FO-WPDRS are demonstrated in Section 5. An FOWPT prototype is built to prove the viability of the proposed method, the experimental results on the characteristics of the FOC and the performance of applying FOC to WPT are presented and discussed in Section 6. Finally, a conclusion is drawn in Section 7.

## 2. Fundamental Analysis of FOEs

This section presents the fundamental analysis of FOEs. A series-connected fractional-order  $RL_\beta C_\alpha$  circuit is shown in Figure 1.

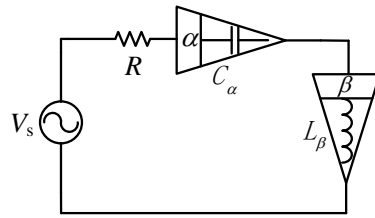


**Figure 1.** Schematic of fractional-order  $RL_\beta C_\alpha$  circuit.

The current-voltage relationship of fractional-order capacitor is defined as [27]

$$i(t) = C_\alpha \frac{d^\alpha v(t)}{dt^\alpha}, \quad (1)$$

where  $d^\alpha/dt^\alpha$  is termed as the fractional-order derivative,  $v(t)$  is the capacitor voltage,  $i(t)$  is the capacitor current,  $\alpha$  ( $0 < \alpha < 2$ ) is the order of the capacitor and  $C_\alpha$  is the capacitance expressed in  $F/s^{1-\alpha}$ . The impedance of FOC can be derived from Equation (1) and expressed as  $Z_C(s) = 1/(s^\alpha C_\alpha)$ , where  $s$  is the Laplace operator. With  $s = j\omega$ , the impedance can be represented by the following equation.

$$Z_C(j\omega) = \frac{1}{(j\omega)^\alpha C_\alpha} = \frac{1}{\omega^\alpha C_\alpha} (\cos(\frac{\alpha\pi}{2}) - j \sin(\frac{\alpha\pi}{2})), \quad (2)$$

where  $\omega$  is the angular frequency. Similarly, the impedance of fractional-inductor can be expressed as Equation (3).

$$Z_L(j\omega) = (j\omega)^\beta L_\beta = \omega^\beta L_\beta (\cos(\frac{\beta\pi}{2}) + j \sin(\frac{\beta\pi}{2})), \quad (3)$$

where  $\beta$  ( $0 < \beta < 2$ ) is the order of the inductor and  $L_\beta$  is the inductance. In terms of Equations (2) and (3), the impedance of the FOEs includes real part and imaginary part, while the conventional ones only have the imaginary part.

As shown in Figure 2, the order of FOEs varies from  $-2$  to  $2$ , which means that the phase falls in  $(-\pi, \pi)$ . It can be noted that that FOEs become integer elements if  $\alpha(\beta) \rightarrow 1$ ; when  $\alpha(\beta) \rightarrow 2$  on the other hand, the circuit works as a second-order system.

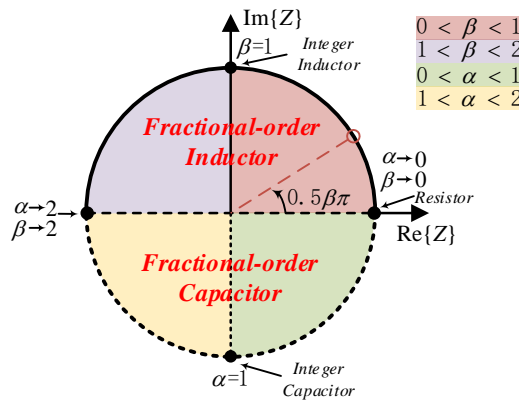


**Figure 2.** Fractional-order elements.

According to the phasor diagram shown in Figure 3, FOEs act as power-consuming elements with  $1 < \alpha < 2$  or  $1 < \beta < 2$  where it has the characteristic of a negative resistor and supplies power.

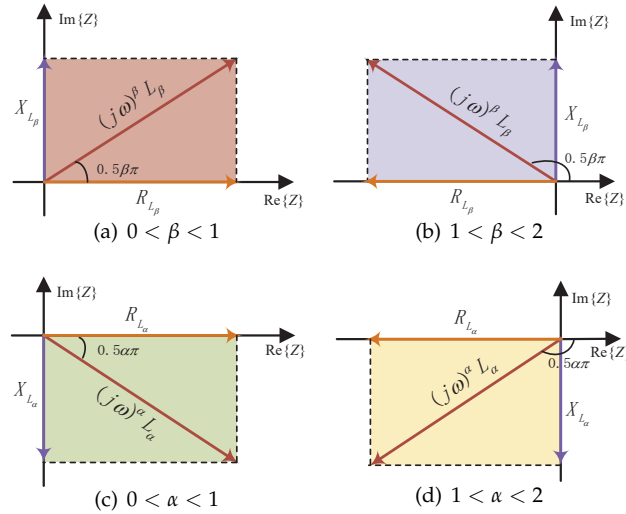


Figure 3. Phasor diagram.

### 3. Modeling the Proposed FO-WPT Strategy

In this section, an FO-WPT model is established and the relationships of fractional resonant frequency, efficiency and output power are derived.

The schematic of FO-WPT is shown in Figure 4a, where the dashed circuit of Figure 4a shows the coil-to-coil resonators, with the detailed model depicted in Figure 4b. In Figure 4a, the primary circuit consists of a high-frequency voltage source  $V_s$ , an FOC  $C_{\alpha_1}$  whose order is  $\alpha_1$ , a fractional-order inductor (FOI)  $L_{\beta_1}$  with order  $\beta_1$  and a primary resistor  $R_1$ . On the secondary side, it is composed of an FOI  $L_{\beta_2}$  with an order  $\beta_2$ , an FOC  $C_{\alpha_2}$  with an order  $\alpha_2$  and resistor  $R_2$ . Term  $M_\gamma$  is the mutual inductance whose order is  $\gamma$  and  $R_L$  represents an equivalent resistance of the load. Then, one can describe the corresponding equation as in Equation (4).

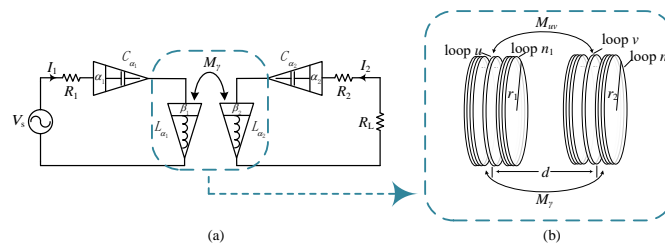


Figure 4. (a) Schematic of FO-WPT and (b) its coil-to-coil model.

$$\begin{bmatrix} Z_{f_1} & (j\omega)^{\gamma_{12}} M_{\gamma_{12}} \\ (j\omega)^{\gamma_{21}} M_{\gamma_{21}} & R_L + Z_{f_2} \end{bmatrix} \cdot \begin{bmatrix} I_1 \\ I_2 \end{bmatrix} = \begin{bmatrix} V_s \\ 0 \end{bmatrix}, \quad (4)$$

where  $M_{\gamma_{12}} = M_{\gamma_{21}} = M_\gamma$  is the mutual inductance between winding-1 and winding-2,  $\gamma_{12} = \gamma_{21} = \gamma$  is the order of mutual inductance,  $Z_{f_n} = R_n + (j\omega)^{\beta_n} L_{\beta_n} + 1/((j\omega)^{\alpha_n} C_{\alpha_n})$  ( $n = 1, 2$ ).

To simplify the analysis, a system with two coaxial circular filamentary current windings are taken as an example for FO-WPT in this study. Maxwell has derived a well-known equation to calculate the mutual inductance. Then, one can obtain the mutual inductance of a pair of single circular loops (loop  $u$  and loop  $v$ , as shown in Figure 4b) as

$$M_{uv} = \mu_0 \frac{\sqrt{r_1 r_2}}{g} [(2 - g^2) \mathbf{K}(g) - 2 \mathbf{E}(g)], \quad (5)$$

where

$$g = \frac{4r_1 r_2}{d^2 + (r_1 + r_2)^2}, \quad (6)$$

where  $r_1$ ,  $r_2$ , and  $d$  are the radius of loop  $u$ , loop  $v$ , and the distance between them, respectively.  $K(g)$  and  $E(g)$  are the first and second kind corresponding complete elliptic integrals. For two coaxial circular thin-wall windings, the mutual inductance can be calculated by

$$M_\gamma = \sum_{u=1}^{n_1} \sum_{v=1}^{n_2} M_{uv}. \quad (7)$$

In terms of Equation (4), currents in primary side and secondary side are

$$\begin{cases} I_1 = \frac{(Z_{f_2} + R_L)V_s}{Z_{f_1}(Z_{f_2} + R_L) - (j\omega)^{\gamma_{12} + \gamma_{21}} M_{\gamma_{12}} M_{\gamma_{21}}}, \\ I_2 = \frac{(j\omega)^{\gamma_{21}} M_{\gamma_{21}} V_s}{Z_{f_1}(Z_{f_2} + R_L) - (j\omega)^{\gamma_{12} + \gamma_{21}} M_{\gamma_{12}} M_{\gamma_{21}}}. \end{cases} \quad (8)$$

Then the output power of FO-WPT can be calculated by Equation (9), which is shown at the top of the next page, where  $A = Re[Z_{f_1}]$ ,  $B = Im[Z_{f_1}]$ ,  $C = Re[Z_{f_2}] + R_L$ , and  $D = Im[Z_{f_2}]$ .

$$\begin{aligned} P_o &= |I_2|^2 R_L = \left| \frac{(j\omega)^{\gamma_{21}} M_{\gamma_{21}} V_s}{Z_{f_1}(Z_{f_2} + R_L) - (j\omega)^{\gamma_{12} + \gamma_{21}} M_{\gamma_{12}} M_{\gamma_{21}}} \right|^2 R_L \\ &= \frac{\omega^{2\gamma_{12}} M_{\gamma_{12}}^2 R_L V_s^2}{\left[ AC - BD - \omega^{\gamma_{12} + \gamma_{21}} M_{\gamma_{12}} M_{\gamma_{21}} \cos\left(\frac{\gamma_{12} + \gamma_{21}}{2}\pi\right) \right]^2 + \left[ BC + DA - \omega^{\gamma_{12} + \gamma_{21}} M_{\gamma_{12}} M_{\gamma_{21}} \sin\left(\frac{\gamma_{12} + \gamma_{21}}{2}\pi\right) \right]^2}, \end{aligned} \quad (9)$$

In terms of Equation (4), complex power of winding-1 and winding-2 are expressed as

$$S_{f_1} = V_s I_1^* = Z_{f_1} I_1^2 + (j\omega)^{\gamma_{12}} M_{\gamma_{12}} I_2 I_1^*, \quad (10)$$

and

$$S_{f_2} = 0 = (j\omega)^{\gamma_{21}} M_{\gamma_{21}} I_1 I_2^* + (Z_{f_2} + R_L) I_2^2, \quad (11)$$

where  $I_1^*$  and  $I_2^*$  are conjugates of  $I_1$  and  $I_2$ , respectively.

In terms of Equation (3), the expression of fractional-order mutual inductance  $Z_{M_\gamma}$  can be written as

$$Z_{M_\gamma} = (j\omega)^\gamma M_\gamma = \omega^\gamma M_\gamma (\cos(\frac{\gamma\pi}{2}) + j \sin(\frac{\gamma\pi}{2})). \quad (12)$$

Substituting Equation (12) into Equations (10) and (11) yields

$$\begin{aligned} S_{f_1} &= V_s I_1^* \\ &= Z_{f_1} I_1^2 + \omega^{\gamma_{12}} M_{\gamma_{12}} (\cos(\frac{\gamma_{12}\pi}{2}) + j \sin(\frac{\gamma_{12}\pi}{2})) I_2 I_1^*, \end{aligned} \quad (13)$$

and

$$\begin{aligned} S_{f_2} &= \omega^{\gamma_{21}} M_{\gamma_{21}} (\cos(\frac{\gamma_{21}\pi}{2}) \\ &\quad + j \sin(\frac{\gamma_{21}\pi}{2})) I_1 I_2^* + (Z_{f_2} + R_L) I_2^2 = 0. \end{aligned} \quad (14)$$

Rewrite Equation (14) as

$$\begin{aligned} & -j\omega^{\gamma_{21}} M_{\gamma_{21}} \sin\left(\frac{\gamma_{21}\pi}{2}\right) I_1 I_2^* \\ & = \omega^{\gamma_{21}} M_{\gamma_{21}} \cos\left(\frac{\gamma_{21}\pi}{2}\right) I_1 I_2^* + (Z_{f_2} + R_L) I_2^2 \\ & = (j\omega^{\gamma_{21}} M_{\gamma_{21}} \sin\left(\frac{\gamma_{21}\pi}{2}\right)) I_1^* I_2^*, \end{aligned} \quad (15)$$

then, substituting Equation (15) into Equation (13) results in

$$\begin{aligned} & V_s I_1^* \\ & = Z_{f_1} I_1^2 + (Z_{f_2}^* + R_L) I_2^2 + 2 \cdot \omega^{\gamma_{21}} M_{\gamma_{21}} \cos\left(\frac{\gamma_{12}\pi}{2}\right) I_1^* I_2 \\ & = Z_{f_1} I_1^2 + (Z_{f_2}^* + R_L) I_2^2 + 2 \cdot \text{Re}[(j\omega)^{\gamma_{12}} M_{\gamma_{12}}] \cdot I_1^* I_2. \end{aligned} \quad (16)$$

Then, one can obtain the FO-WPT efficiency as

$$\eta = \frac{R_L |I_2|^2}{\text{Re}[V_s I_1^*]}. \quad (17)$$

#### 4. An Example: Fractional-Order Wireless Power Domino-Resonators System

In [19], Zhong, who has considered the effect of nonadjacent resonators, established a Wireless Power Domino-Resonator Systems and found that the maximum efficiency operation slightly shifted away from the resonant frequency of the resonators. In this section, an FO-WPDRS, which is equipped with FOEs, is derived from the model proposed by Zhong and its schematic is shown in Figure 5. A general model of FO-WPDRS is depicted in Figure 6.

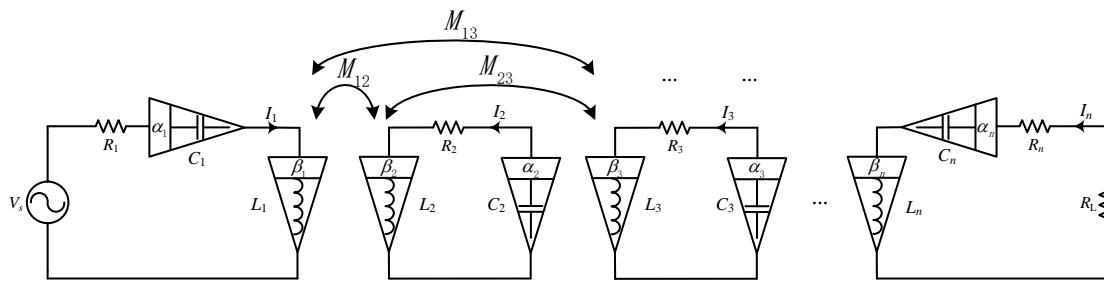


**Figure 5.** Schematic of FO-WPDRS.

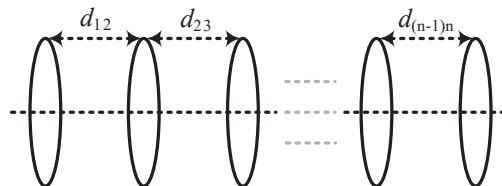


**Figure 6.** General model of domino-system with  $n$  resonators.

$$\begin{bmatrix}
Z_{f_1} & (j\omega)^{\gamma_{12}} M_{12} & (j\omega)^{\gamma_{13}} M_{13} & \cdots & \cdots & (j\omega)^{\gamma_{1n}} M_{1n} \\
(j\omega)^{\gamma_{21}} M_{21} & Z_{f_2} & (j\omega)^{\gamma_{23}} M_{23} & \cdots & \cdots & (j\omega)^{\gamma_{2n}} M_{2n} \\
\vdots & \vdots & \vdots & \ddots & \vdots & \vdots \\
(j\omega)^{\gamma_{(n-1)1}} M_{(n-1)1} & \cdots & \cdots & & Z_{f_{n-1}} & (j\omega)^{\gamma_{(n-1)n}} M_{(n-1)n} \\
(j\omega)^{\gamma_{n1}} M_{n1} & \cdots & \cdots & & (j\omega)^{\gamma_{n(n-1)}} M_{n(n-1)} & R_L + Z_{f_n}
\end{bmatrix} \cdot \begin{bmatrix} I_1 \\ I_2 \\ \vdots \\ I_{n-1} \\ I_n \end{bmatrix} = \begin{bmatrix} V_s \\ 0 \\ \vdots \\ 0 \\ 0 \end{bmatrix} \quad (18)$$

The circuit equation is expressed in Equation (18), as shown at the top of the next page, where  $M_{ij}$  ( $i \neq j$ ) is the mutual inductance between winding- $i$  and winding- $j$ ,  $R_L$  is the load resistance which is connected to winding- $n$  and  $Z_{f_i} = R_i + (j\omega)^{\beta_i} L_i + 1 / ((j\omega)^{\alpha_i} C_i)$  ( $i = 1, 2, \dots, n$ ). Other variables are listed as follows:

- $I_i$  is the current in winding- $i$ ,
- $L_i$  is the fractional-order inductance of winding- $i$ ,
- $C_i$  is the fractional-order capacitance of winding- $i$ ,
- $R_i$  is the resistance of winding- $i$ ,
- $\alpha_i$  is the order of FOC in winding- $i$ ,
- $\beta_i$  is the order of FOI in winding- $i$ ,
- $\gamma_{ij}$  is the order of mutual inductance  $M_{ij}$  and  $M_{ij} = M_{ji}$ ,
- $\omega$  is angular frequency.

Then, the total complex power of the system reads

$$S_{\text{total}} = V_s I_1^* = Z_{f_1} |I_1|^2 + \sum_{m=2}^n (j\omega)^{\gamma_{1m}} M_{1m} I_m I_1^*. \quad (19)$$

The complex power of winding- $i$  ( $i \geq 2$ ) can generally be written as

$$\begin{aligned}
S_{f_i} &= Z_{f_i} |I_i|^2 + \sum_{m=1}^i (j\omega)^{\gamma_{mi}} M_{mi} I_m I_i^* + \sum_{l=i+1}^n (j\omega)^{\gamma_{il}} M_{il} I_l I_i^* \\
&= 0,
\end{aligned} \quad (20)$$

where  $I_i^*$  is the conjugate of current  $I_i$ .

Then, Equation (20) can be rewritten as

$$\begin{aligned}
&- j\omega^{\gamma_{i1}} M_{i1} \sin\left(\frac{\gamma_{i1}\pi}{2}\right) I_1 I_i^* \\
&= Z_{f_i} |I_i|^2 + \omega^{\gamma_{i1}} M_{i1} \cos\left(\frac{\gamma_{i1}\pi}{2}\right) I_1 I_2^* \\
&\quad + \sum_{m=2}^i (j\omega)^{\gamma_{mi}} M_{mi} I_m I_i^* + \sum_{l=i+1}^n (j\omega)^{\gamma_{il}} M_{il} I_l I_i^* \\
&= (j\omega^{\gamma_{i1}} M_{i1} \sin\left(\frac{\gamma_{i1}\pi}{2}\right)) I_1^* I_i^*.
\end{aligned} \quad (21)$$

Substituting Equation (21) into Equation (22) results in

$$\begin{aligned}
 S_{\text{total}} &= V_s I_1^* \\
 &= Z_{f_1} |I_1|^2 + R_L |I_n|^2 + \sum_{m=2}^n I_m^2 Z_{f_m}^* \\
 &\quad + 2 \cdot \sum_{m=2}^n \operatorname{Re}[(j\omega)^{\gamma_{1m}} M_{1m}] I_m I_1^* \\
 &\quad + 2 \cdot \sum_{l=2}^{n-1} \sum_{m=l+1}^n \operatorname{Re}[I_l^* I_m] \cdot (j\omega)^{\gamma_{lm}} M_{lm},
 \end{aligned} \tag{22}$$

where  $Z_{f_m}^*$  is the conjugate of  $Z_{f_m}$ .

Therefore, the real power  $P$  is

$$\begin{aligned}
 P &= \operatorname{Re}[S_{\text{total}}] \\
 &= R_L |I_n|^2 + \sum_{m=1}^n I_m^2 (R_m + \omega^{\beta_m} L_m \cos(\frac{\beta_m \pi}{2}) + \frac{\cos(\frac{\alpha_m \pi}{2})}{\omega^{\alpha_m} C_m}) \\
 &\quad + 2 \cdot \sum_{m=2}^n \omega^{\gamma_{1m}} M_{1m} \cos(\frac{\gamma_{1m} \pi}{2}) \cdot \operatorname{Re}[I_m I_1^*] \\
 &\quad + 2 \cdot \sum_{l=2}^{n-1} \sum_{m=l+1}^n \operatorname{Re}[I_l^* I_m] \cdot \omega^{\gamma_{lm}} M_{lm} \cos(\frac{\gamma_{lm} \pi}{2}).
 \end{aligned} \tag{23}$$

Furthermore, its efficiency is

$$\eta = \frac{R_L |I_n|^2}{P}. \tag{24}$$

## 5. Output Characteristics of FO-WPDRS

Based on the aforementioned analysis, the output characteristics of FO-WPDRS are discussed in this section. In order to simplify the analysis, we denote the distance between adjacent resonators as  $d_{12} = d_{23} = \dots = d_{(n-1)n}$ , and assign parameters of each practical resonator as follows in the numerical analysis.

- fractional-order inductance:  $L_{\beta_i} = L_\beta$ ,
- fractional-order capacitance:  $C_{\alpha_i} = C_\alpha$ ,
- fractional-order mutual inductance:  $M_{ij} = M_{ji} = M$  ( $i \neq j$ ),
- resistance of winding- $i$ :  $R_i = R$ ,
- order of FOI:  $\beta_i = \beta$ ,
- order of FOC:  $\alpha_i = \alpha$ ,
- order of fractional-order mutual inductance:  $\gamma_{ij} = \gamma_{ji} = \gamma = \beta$ .

Numerical analyses were conducted based on the parameters listed in Table 1, and the corresponding results and analyses are presented below.

**Table 1.** Simulation Parameters.

Parameter	Value
Voltage source $V_s$	50 V
Inductance $L_\beta$	90.7 $\mu\text{H}$
Capacitance $C_\alpha$	1.036 nF
Resistance of winding- $i$ $R$	0.9 $\Omega$
Mutual inductance $M$	2.85 $\mu\text{H}$
Separation $d_{(n-1)n}$	0.3 m
Load resistance $R_L$	10 $\Omega$

### 5.1. Fractional Orders of $\alpha$ and $\beta$ to Improve Resonant Frequency

The resonant frequency of FO-WDPRS is described in Equation (25), while the resonant frequency of the traditional WPT ( $\alpha = \beta = \gamma = 1$ ) is presented in Equation (26).

$$f_{\text{frac}} = \frac{1}{2\pi} \left[ \frac{\sin(\alpha\pi/2)}{L_\beta C_\alpha \sin(\beta\pi/2)} \right]^{\frac{1}{\alpha+\beta}} \quad (25)$$

$$f_{\text{trad}} = \frac{1}{2\pi} \frac{1}{\sqrt{L_\beta C_\alpha}} = 520 \text{ kHz} \quad (26)$$

According to Figure 7, relevant remarks about the resonant frequency of FO-WDPRS are made as follows:

- $\alpha$  and  $\beta$  are a pair of symmetric parameters which have the same impact on the resonant frequency.
- As depicted in Figure 7a, it is found that  $\lg \frac{f_{\text{frac}}}{f_{\text{trad}}} \gg 0$  ( $Z \gg 0$ ), which means that when  $\alpha < 1$  and  $\beta < 1$ , the resonant frequency FO-WDPRS will dramatically increase with an increased  $\alpha(\beta)$  compared to the traditional one.
- As shown in Figure 7b,c, it is noted that  $\lg \frac{f_{\text{frac}}}{f_{\text{trad}}} < 0$  ( $Z < 0$ ) in some regions of the  $\alpha$ - $\beta$  plane, implying that the resonant frequency of FO-WDPRS can be reduced.
- Similarly, it is found that  $\lg \frac{f_{\text{frac}}}{f_{\text{trad}}} < 0$  ( $Z < 0$ ) in Figure 7d, which implies that the resonant frequency of FO-WDPRS can be lowered if we set  $1 < \alpha < 2, 1 < \beta < 2$ .
- To describe the impact of  $\alpha$  and  $\beta$  on resonant frequency, Figure 7a–d are collocated in Figure 7e to find the detailed range of  $\alpha$  and  $\beta$  for  $f_{\text{frac}} > f_{\text{trad}}$  and  $f_{\text{frac}} < f_{\text{trad}}$ , respectively. Hence, one can choose the appropriate  $\alpha$  and  $\beta$  to realize the desired frequency.

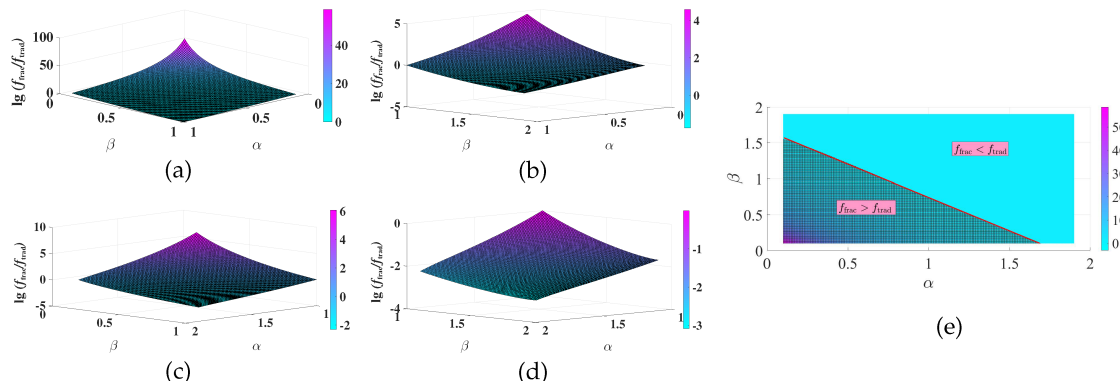


**Figure 7.** Relationship curves among  $\alpha$ ,  $\beta$ , and  $\lg \frac{f_{\text{frac}}}{f_{\text{trad}}}$ : Variations of  $0 < \alpha < 2$  and  $0 < \beta < 2$ . In detail, sub-figures demonstrate the details of 3D plots of (a)  $0 < \alpha < 1, 0 < \beta < 1$ , (b)  $0 < \alpha < 1, 1 < \beta < 2$ , (c)  $1 < \alpha < 2, 0 < \beta < 1$ , (d)  $1 < \alpha < 2, 1 < \beta < 2$ , (e)  $0 < \alpha < 2, 0 < \beta < 2$  (Top view). [Note: the resonant frequency of fractional-order WPT is normalized by the traditional one, and the logarithm of normalized value based on 10,  $\lg \frac{f_{\text{frac}}}{f_{\text{trad}}}$ , is taken as Z axis.]

## 5.2. Fractional Orders of $\alpha$ and $\beta$ to Improve Output Power and Efficiency

To study the effect of fractional-order inductors, capacitors and mutual inductors on the output power and efficiency of FO-WPDRS, 3-dimension (3D) plots of the relations among  $\alpha$ ,  $\beta$ ,  $P_o$  and efficiency  $\eta$  are depicted in Figures 8 and 9, respectively. (Note: all the systems operate at the resonant frequency.)

According to Figure 8a–d, it is obvious that there is a resonance point with the maximum output power in all cases. From the simulation results, it can be concluded that the output power of the above FO-WPDRS is greater than the traditional WPT ( $\alpha = \beta = \gamma = 1$ ), which further validates the effectiveness of the proposed FOE method in increasing the output power.

Compared with Figure 9a–e, it is clear that the efficiency of FO-WPDRS, whose average distance between two adjacent resonators is 0.3 m, is higher than the ones with the optimized loads, frequencies and distances or only loads in [19].

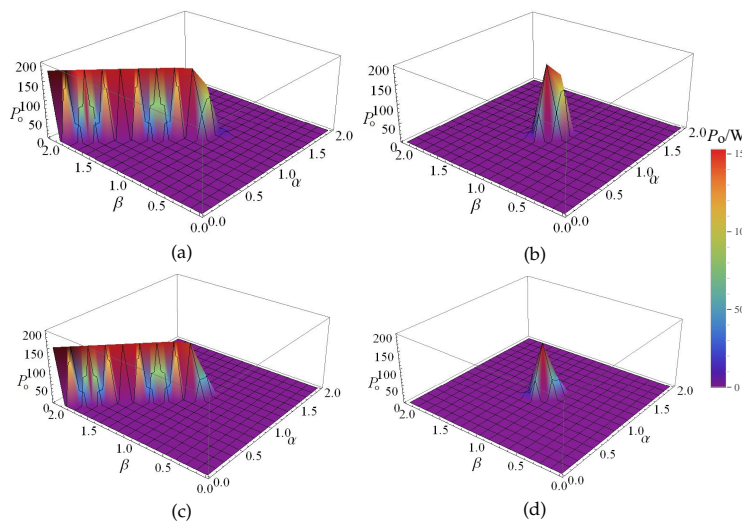


**Figure 8.** Relationship curves among  $\alpha$ ,  $\beta$ , and  $P_o$ : Variations of  $0 < \alpha < 2$  and  $0 < \beta < 2$ . In detail, sub-figures demonstrate the details of 3D plots of (a) FO-WPDRS with 3 resonators, (b) FO-WPDRS with 4 resonators, (c) FO-WPDRS with 5 resonators, and (d) FO-WPDRS with 6 resonators.

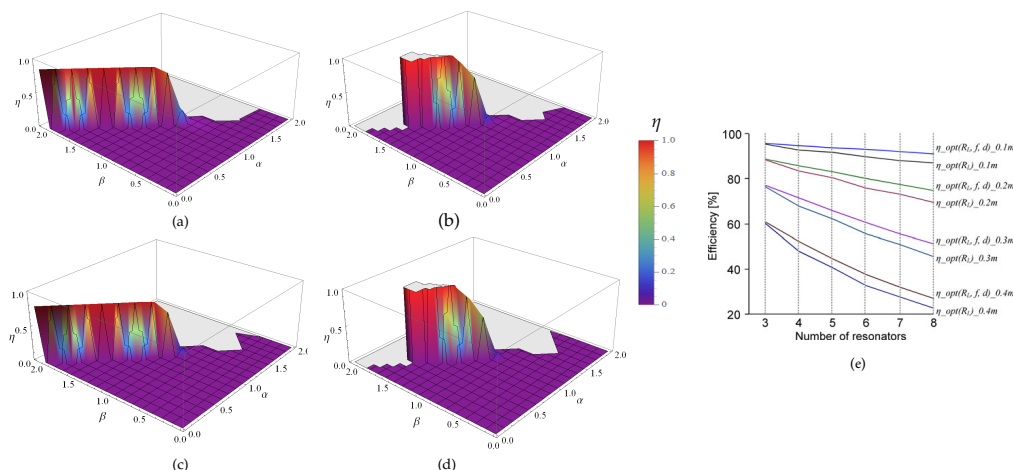


**Figure 9.** Relationship curves among  $\alpha$ ,  $\beta$ , and  $\eta$ : Variations of  $0 < \alpha < 2$  and  $0 < \beta < 2$ . In detail, sub-figures demonstrate the details of 3D plots of (a) FO-WPDRS with 3 resonators, (b) FO-WPDRS with 4 resonators, (c) FO-WPDRS with 5 resonators, (d) FO-WPDRS with 6 resonators and (e) Efficiency comparison between the domino systems with optimized loads, frequencies and distance ( $\eta_{opt}(R_L, f, d)$ ) and the equally spaced systems operating at resonant frequency and with only optimized loads ( $\eta_{opt}(R_L)$ ) with four different average distances: 0.1 m, 0.2 m, 0.3 m, and 0.4 m in [19].

## 6. Simulations and Experiments

Two experimental setups are established in this study to examine the performance of the proposed FO-WPT mechanism: (1) the FOC is powered by a high-frequency power source for the observation of the order of the FOC, and (2) incorporate the FOC built in (1) into the FO-WPT for performance validation. Detailed measurements and analyses are presented follows.

The theoretical analyses in Sections 4 and S4 studied FOCs with a range of orders. In this section, we build a prototype of an FOC with an order of 0.54 to realize the WPT. Please note that it is of significant technical difficulty to manufacture an FOC with an order higher than one. With the facilities available in our laboratory, we only use the FOC of  $0 < \alpha < 1$  to validate our theory. Building FOCs with orders greater than 1 is to be conducted in our future work.

### 6.1. Implementation of Fractional-Order Capacitor

A practical FOC is implemented as depicted in Figure 10 based on Ref. [28]. To realize fractional order  $\alpha = 0.54$ , the corresponding parameters are:  $R_1 = 10 \text{ k}\Omega$ ,  $R_2 = 3.3 \text{ k}\Omega$ ,  $R_3 = 1.0 \text{ k}\Omega$ ,  $R_4 = 330 \Omega$ ,  $R_5 = 100 \Omega$ ,  $C_1 = 1.0 \mu\text{F}$ ,  $C_2 = 470 \text{ nF}$ ,  $C_3 = 330 \text{ nF}$ ,  $C_4 = 220 \text{ nF}$ ,  $C_5 = 100 \text{ nF}$ ,  $R_p = 22 \text{ k}\Omega$ ,  $C_p = 100 \text{ nF}$ .

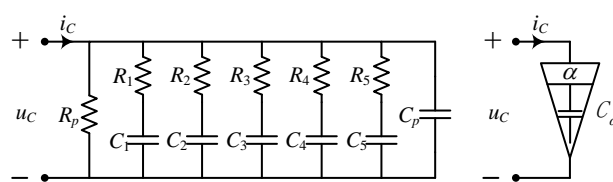


**Figure 10.** Schematic of the FOC.

To further demonstrate the characteristics of the designed FOC, dynamic behavior of the FOC is tested and the corresponding resultant waveforms are shown in Figure 11. Therein, the actual order  $\alpha$  can be obtained by measuring the phase difference between the input voltage and current. As seen in Figure 11, the input current  $i_C$  has a leading phase angle of  $48.6^\circ$  from the input voltage  $u_C$ , and the actual order  $\alpha$  is thus 0.54.

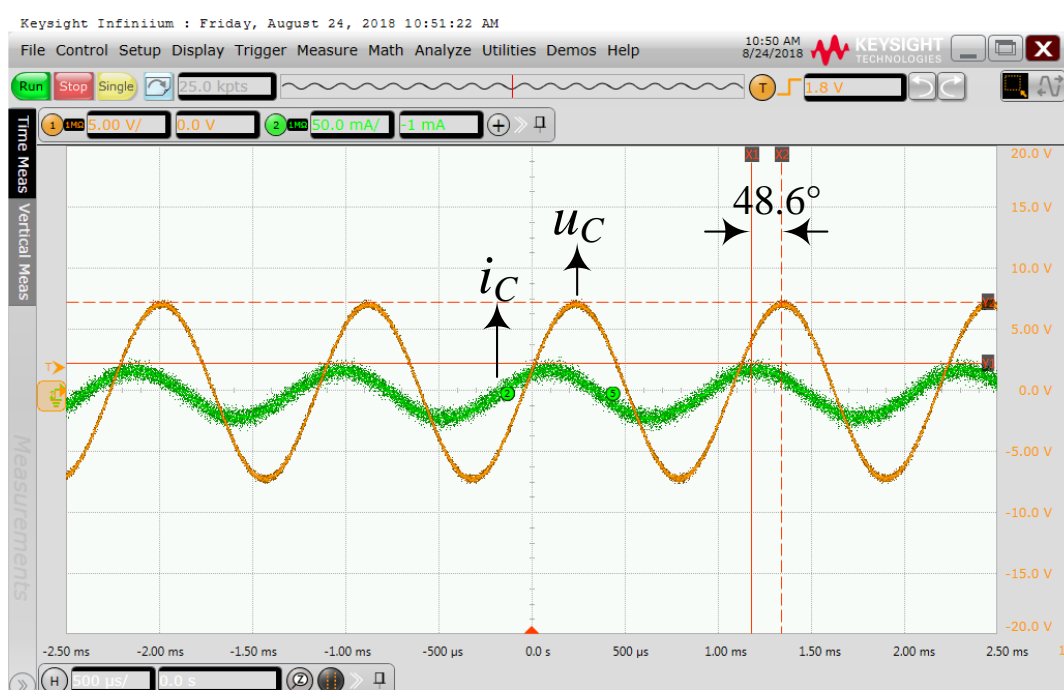


**Figure 11.** Experimental waveforms of FOC.

## 6.2. FO-WPT with the Constructed FOC

In this subsection, a prototype of FO-WPT with the constructed FOC is presented in Figure 12, and the corresponding simulation and experimental waveforms are shown in Figures 13 and 14, respectively. The distance between the transmitter and receiver is 0.3 m. It can be seen that FO-WPT is in resonance since the current  $i_R$  and voltage  $u_R$  have the same phase angle, which indicates a unity power factor, representing the best power use, i.e., a higher energy efficiency. This experiment together with the simulation studies shown before corroborates the advantages of the proposed FO-WPT with fractional order elements, which have more favorable output characteristics and higher energy transfer efficiency.

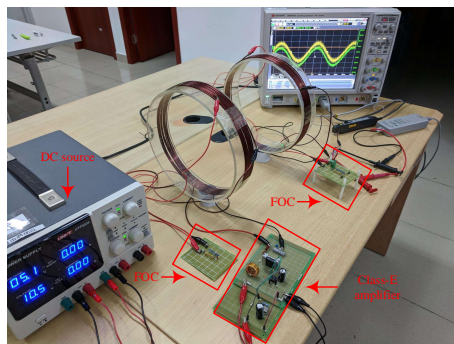


**Figure 12.** Experimental prototype of the FO-WPT.

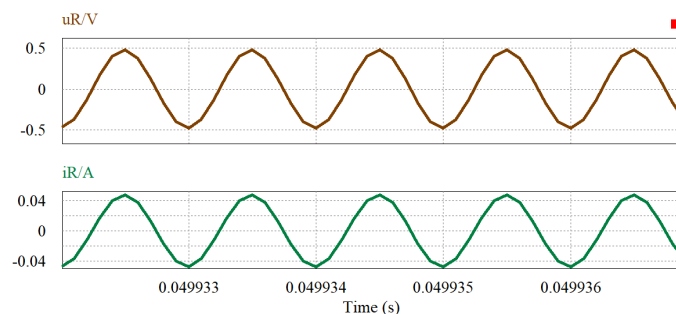


**Figure 13.** Simulation waveforms of FO-WPT.

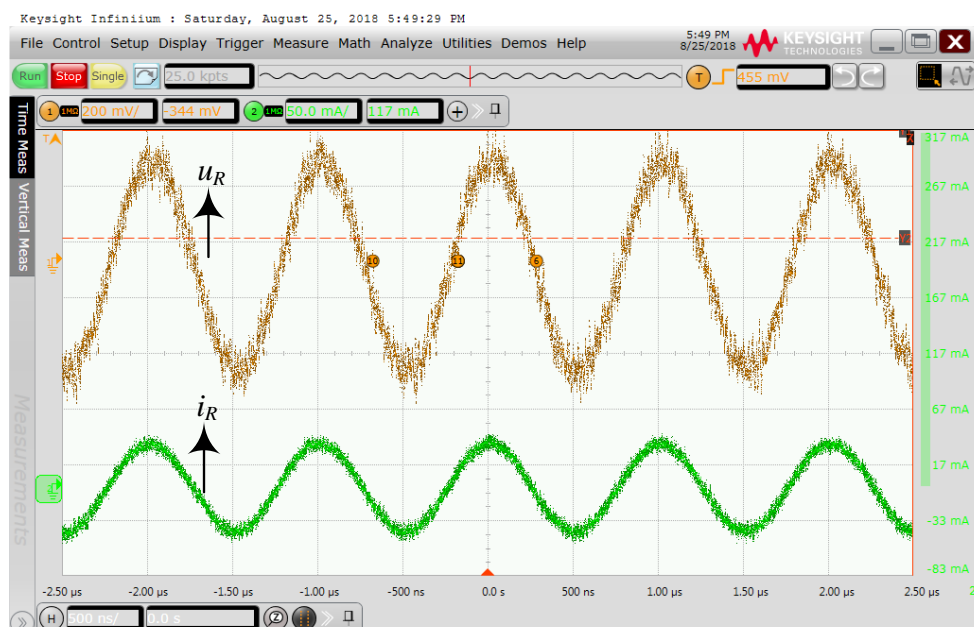


**Figure 14.** Experimental waveforms of FO-WPT.

It is obvious that the experimental results well agree with the simulations and theoretical analyses according to the figures, it is found that there a little voltage drop in experimental one due to the parasitic parameters of the components.

## 7. Conclusions

In this study, we proposed a novel fractional-order circuit elements-based wireless power transmission solution, aiming to reduce the resonant frequency and improving the output power quality and efficiency. Detailed mathematical modeling of the proposed FO-WPT has been presented. Simulation studies of a typical example FO-WPDRS validated the theoretical analysis, and shown reduced frequency, improved efficiency and enhanced output power. An experimental prototype has been developed to validate the proposed method, and the results are corresponding with the analyses. This work could lay a solid foundation for further investigations in fractional-order elements-based WPT solutions, which may lead to wide industrial applications in wireless power transfer.

**Author Contributions:** Conceptualization, G.Z. and Z.O.; methodology, G.Z. and Z.O.; software, Z.O.; validation, G.Z. and Z.O.; formal analysis, L.Q.; investigation, Z.O.; writing—original draft preparation, Z.O.; writing—review and editing, G.Z.; supervision, G.Z.; project administration, L.Q.; funding acquisition, L.Q.

**Funding:** This research was funded by [National Natural Science Foundation of China] grant numbers [51907032, U1501251, 51277030, 61733015], [Natural Science Foundation of Guangdong Province] grant numbers [2017A030310243, 2018A030313365] and [Science and Technology Planning Project of Guangzhou] grant number [201804010310].

**Conflicts of Interest:** The authors declare no conflict of interest.

## References

1. Jiang, W.; Xu, S.; Li, N.; Lin, Z.; Williams, B.W. Wireless power charger for light electric vehicles. In Proceedings of the IEEE 11th International Conference on Power Electronics and Drive Systems, Sydney, Australia, 9–12 June 2015; pp. 562–566.
2. Yang, Q.; Zhang, P.; Zhu, L.; Xue, M.; Zhang, X.; Li, Y. Key fundamental problems and technical bottlenecks of the wireless power transmission technology. *Trans. China Electrotech. Soc.* **2015**, *30*, 1–8.
3. Musavi, F.; Wilson, E. Overview of wireless power transfer technologies for electric vehicle battery charging. *IET Power Electron.* **2014**, *7*, 60–66. [[CrossRef](#)]
4. Liu, X.; Wang, G.; Ding, W. Efficient circuit modelling of wireless power transfer to multiple devices. *IET Power Electron.* **2014**, *7*, 3017–3022. [[CrossRef](#)]
5. Almohaimed, A.; Amaya, R.; Lima, J. An adaptive power harvester with active load modulation for highly efficient short/long range RF WPT applications. *Electronics* **2018**, *7*, 125. [[CrossRef](#)]
6. Lu, G.; Shi, L.; Ye, Y. Maximum Throughput of TS/PS Scheme in an AF Relaying Network With Non-Linear Energy Harvester. *IEEE Access* **2018**, *6*, 26617–26625. [[CrossRef](#)]
7. Kurs, A.; Karalis, A.; Moffatt, R.; Joannopoulos, J.D.; Fisher, P.; Soljačić, M. Wireless power transfer via strongly coupled magnetic resonances. *Science* **2007**, *317*, 83–86. [[CrossRef](#)] [[PubMed](#)]
8. Nottiani, D.G.; Leccese, F. A simple method for calculating lumped parameters of planar spiral coil for wireless energy transfer. In Proceedings of the 11th International Conference on Environment and Electrical Engineering, Venice, Italy, 18–25 May 2012; pp. 869–872.
9. Houran, M.; Yang, X.; Chen, W. Magnetically Coupled Resonance WPT: Review of Compensation Topologies, Resonator Structures with Misalignment, and EMI Diagnostics. *Electronics* **2018**, *7*, 296. [[CrossRef](#)]
10. Liu, X.; Liu, J.; Wang, J.; Wang, C.; Yuan, X. Design Method for the Coil-System and the Soft Switching Technology for High-Frequency and High-Efficiency Wireless Power Transfer Systems. *Energies* **2017**, *11*, 7. [[CrossRef](#)]
11. Wang, T.; Liu, X.; Jin, N. Wireless Power Transfer for Battery Powering System. *Electronics* **2018**, *7*, 178. [[CrossRef](#)]
12. Zhang, W.; Mi, C.C. Compensation topologies of high-power wireless power transfer systems. *IEEE Trans. Veh. Tech.* **2016**, *65*, 4768–4778. [[CrossRef](#)]

13. He, X.; Shu, W.; Yu, B.; Ma, X. Wireless Power Transfer System for Rotary Parts Telemetry of Gas Turbine Engine. *Electronics* **2018**, *7*, 58. [[CrossRef](#)]
14. Rong, C.; Tao, X.; Lu, C.; Hu, Z.; Huang, X.; Zeng, Y.; Liu, M. Analysis and Optimized Design of Metamaterials for Mid-Range Wireless Power Transfer Using a Class-E RF Power Amplifier. *Appl. Sci.* **2019**, *9*, 26. [[CrossRef](#)]
15. Hernández Robles, I.A.; Lozano García, J.M.; Martínez Juárez, J.J. Simulation for Obtaining Relevant Parameters for Optimal Wireless Power Transfer. *Comput. Y Sist.* **2019**, *23*, 81. [[CrossRef](#)]
16. Yin, J.; Lin, D.; Lee, C.K.; Hui, S.R. A systematic approach for load monitoring and power control in wireless power transfer systems without any direct output measurement. *IEEE Trans. Power Electron* **2014**, *30*, 1657–1667. [[CrossRef](#)]
17. Tan, L.; Guo, J.; Huang, X.; Wen, F. Output power stabilisation of wireless power transfer system with multiple transmitters. *IET Power Electron* **2016**, *9*, 1374–1380. [[CrossRef](#)]
18. Syms, R.R.A.; Solymar, L.; Young, I.R.; Floume, T. Thin-film magneto-inductive cables. *J. Phys. D Appl. Phys.* **2010**, *43*, 55102. [[CrossRef](#)]
19. Lee, C.K.; Zhong, W.X.; Hui, S.Y.R. Effects of magnetic coupling of nonadjacent resonators on wireless power domino-resonator systems. *IEEE Trans. Power Electron.* **2012**, *27*, 1905–1916. [[CrossRef](#)]
20. Park, N.; Choi, H.S.; Jeong, I.S.; Choi, H.W. Analysis of efficiency characteristics of superconducting coil-applied wireless power transmission systems by transmission distance. In Proceedings of the 2017 16th International Superconductive Electronics Conference (ISEC), Naples, Italy, 12–16 June 2017; pp. 1–3.
21. Jeong, I.S.; Jung, B.I.; You, D.S.; Choi, H.S. Analysis of S-parameters in magnetic resonance WPT using superconducting coils. *IEEE Trans. Appl. Supercond.* **2016**, *26*, 1–4. [[CrossRef](#)]
22. Chen, L.; Liu, S.; Zhou, Y.C.; Cui, T.J. An optimizable circuit structure for high-efficiency wireless power transfer. *IEEE Trans. Ind. Electron.* **2013**, *60*, 339–349. [[CrossRef](#)]
23. Li, H.; Li, J.; Wang, K.; Chen, W.; Yang, X. A maximum efficiency point tracking control scheme for wireless power transfer systems using magnetic resonant coupling. *IEEE Trans. Power. Electron.* **2015**, *30*, 3998–4008. [[CrossRef](#)]
24. Radwan, A.G.; Shamim, A.; Salama, K.N. Theory of fractional order elements based impedance matching networks. *IEEE Microw. Wirel. Compon. Lett.* **2011**, *21*, 120–122. [[CrossRef](#)]
25. Radwan, A.G.; Shamim, A.; Salama, K.N. Impedance matching through a single passive fractional elemen. In Proceedings of the 2012 IEEE International Symposium on Antennas and Propagation, Chicago, IL, USA, 8–14 July 2012; pp. 1–2.
26. Chen, M.R.; Zeng, G.Q.; Dai, Y.X.; Lu, K.D.; Bi, D.Q. Fractional-Order Model Predictive Frequency Control of an Islanded Microgrid. *Energies* **2019**, *12*, 84. [[CrossRef](#)]
27. Radwan, A.G. Resonance and Quality Factor of the  $RL_{\alpha}C_{\alpha}$  Fractional Circuit. *IEEE J. Emerg. Sel. Top. Circuits Syst.* **2013**, *3*, 377–385. [[CrossRef](#)]
28. Shu, X.; Zhang, B. The Effect of Fractional Orders on the Transmission Power and Efficiency of Fractional-Order Wireless Power Transmission System. *Energies* **2018**, *11*, 1774. [[CrossRef](#)]



© 2019 by the authors. Licensee MDPI, Basel, Switzerland. This article is an open access article distributed under the terms and conditions of the Creative Commons Attribution (CC BY) license (<http://creativecommons.org/licenses/by/4.0/>).